

# ChemComm

Accepted Manuscript



This is an *Accepted Manuscript*, which has been through the Royal Society of Chemistry peer review process and has been accepted for publication.

*Accepted Manuscripts* are published online shortly after acceptance, before technical editing, formatting and proof reading. Using this free service, authors can make their results available to the community, in citable form, before we publish the edited article. We will replace this *Accepted Manuscript* with the edited and formatted *Advance Article* as soon as it is available.

You can find more information about *Accepted Manuscripts* in the [Information for Authors](#).

Please note that technical editing may introduce minor changes to the text and/or graphics, which may alter content. The journal's standard [Terms & Conditions](#) and the [Ethical guidelines](#) still apply. In no event shall the Royal Society of Chemistry be held responsible for any errors or omissions in this *Accepted Manuscript* or any consequences arising from the use of any information it contains.



ChemComm

COMMUNICATION

## Controlling of DNA Origami Inter-tile Connection with Vertical Linkers

Received 00th January 20xx,  
Accepted 00th January 20xx

Risheng Wang<sup>\*abc</sup>, Kent Gorday<sup>d</sup>, Colin Nuckolls<sup>b</sup>, and Shalom J. Wind<sup>\*a</sup>

DOI: 10.1039/x0xx00000x

www.rsc.org/

**This paper describes a new method that enables high yield assembly along both of the two-dimensional edges of DNA origami tiles by controlling of the Mg<sup>2+</sup> concentration; High Mg<sup>2+</sup> concentrations promote linkage connections between the vertical edges of the tiles. As a demonstration, DNA origami dimers assembled from two rectangular origami along the vertical edges are used as scaffolds for the double sided assembly of gold nanoparticles with different inter-particle spacings.**

DNA origami<sup>1</sup> is a two dimensional surface formed by folding a long single-stranded circular DNA (7.2 kb genome of phage M13mp18) with the help of ~220 shorter “staple” strands into different shapes. A square origami tile, made in this way, is limited to ~100 nm on its sides. This size restriction, dictated by the length of the M13mp18 substrate strand, has spurred interest in the further self-assembly of single DNA origami tiles into larger superstructures, typically by association along the origami edges.<sup>2-7</sup> Larger arrays of DNA origami are useful in many applications, including as templates for the nanoscale assembly of metallic nanoparticles/nanorods,<sup>8-11</sup> proteins,<sup>12, 13</sup> carbon nanotubes<sup>14-17</sup> and other functional components.<sup>18-20</sup> Therefore, it is important to understand and control the assembly between tile edges to allow the creation of more perfect arrays and more diverse types of structures. The assembly between two origami edges can either be made between connections that run parallel to the duplex long axis (horizontal) or perpendicular to the duplex axis (vertical). In general, assembly along the vertical axis is difficult, this is because of the strong electrostatic repulsion between negatively charged DNA backbones. Therefore most studies of origami tile assembly have focused on assembly along the

horizontal edges.<sup>4-6</sup> There has been a large effort studying the assembly of DNA origami into 2D arrays using multiple tiles. For example, Liu et al, successfully self-assembled a 2D origami crystal structure with ~2 to 3 μm size by deliberate designed cross-shaped double layer origami unit, which expanded inter-tile connection along the duplex axis (horizontal linkers) in both directions.<sup>5</sup> A DNA origami was designed with four-way connectors to form cruciform and hollow cube structures.<sup>6</sup> In those studies, the helical-axis element of all four edges involved minimal electrostatic repulsion and maximal π-stacking interactions to facilitate the association of DNA origami. In a related study, a nine-piece DNA origami jigsaw, formed by shape and sequence selectivity with horizontal and vertical connectors, gave a low yield of ~30%.<sup>7</sup> These observations suggest that the inter-tile association between DNA origami is favorable along the duplex axis due to the weak electrostatic repulsion and strong π-stacking with the DNA duplex ends. To overcome the limitation of M13mp18, longer single-stranded PCR products<sup>21</sup> and double stranded DNA<sup>22</sup> have been employed as scaffolds to make larger DNA origami structures. Recently, new methods have been developed to create DNA origami arrays, such as surface diffusion assisted assembly,<sup>23</sup> gold nanoparticles bridged super-nanostructures,<sup>24, 25</sup> truchet tiling based combinatorial approach,<sup>26</sup> small DNA tiles used as folding staples<sup>2, 3</sup>, and shape-complementarity mediated organization.<sup>27</sup> Common to these methods is the need for dedicated design of the origami tile or further materials processing. Here we demonstrated that the simple addition of magnesium salts enables efficient assembly along the vertical edges of rectangular origami. As a proof of concept we assemble dimers of rectangular origami into a square using vertical connections (Fig. 1a). Furthermore, we show that each of the corners of the assembled dimer can direct the assembly of multiple gold nanoparticles.

The design of DNA rectangle origami is shown in Fig. 1a, the length of origami tile in the horizontal direction (parallel to the helical axis) is 192 nucleotides. In the vertical direction, (perpendicular to the helical axis) there are 20 parallel helices.

<sup>a</sup> Department of Applied Physics & Applied Mathematics, Columbia University, New York, NY 10027 (USA) E-mail: sw2128@columbia.edu.

<sup>b</sup> Department of Chemistry, Columbia University, New York, NY 10027.

<sup>c</sup> Present address: Department of Chemistry, Missouri University of Science and Technology, Rolla, MO 65409 (USA) E-mail: wangri@mst.edu.

<sup>d</sup> Department of Physics, Missouri University of Science and Technology, Rolla, MO 65409 (USA).

†Electronic Supplementary Information (ESI) available. See DOI: 10.1039/x0xx00000x

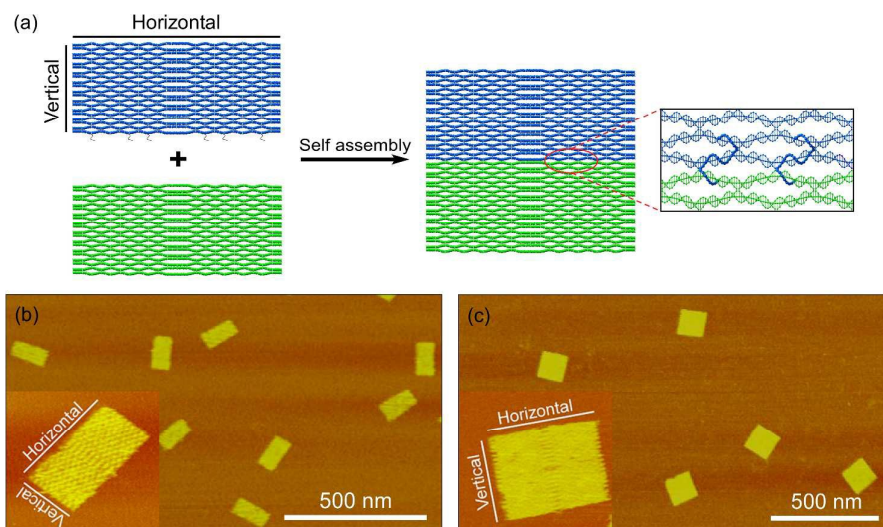


**Fig.1** (a) Schematic illustration of self-assembly of rectangle origami dimer with vertical linkers. (b) AFM image of DNA rectangle monomer. (c) AFM image of DNA rectangle dimer. Both of images were scanned with tapping mode in buffer.

The DNA was folded into a rectangle in a solution containing 40 mM tris buffer (pH 7.6), 2 mM EDTA, and 12.5 mM  $Mg^{2+}$  using the method of Rothemund.<sup>1</sup> Fig. 1b shows an AFM image of the origami rectangles on mica (tapping mode) in buffer. From the AFM micrograph, the average size of rectangle origami is  $\sim 120$  nm by 60 nm and the duplexes run along the long axis (inset of Fig. 1b). When the structures were scanned in the AFM at ambient condition rather than in buffer, the average size of rectangle shrunk to  $\sim 110$  nm  $\times$  45 nm (See Fig. S1).

To assemble the rectangles into dimers, we incorporated six sticky-ended cohesions along the vertical direction of the upper origami in Fig. 1a. The length of vertical linkers is 8 nucleotides, and they are complementary to sequences in the lower rectangle origami. Before the self-assembly process, the two monomers were purified separately to remove the extra helper strands with a 100 kDa MWCO centrifuge filter. After purification, the two complementary monomers were mixed together in an equal molar ratio with varied magnesium concentration and the solution was annealed at 45 °C and allowed to cool to room temperature. The square-shaped DNA rectangle dimer is shown in Fig. 1c. The size of the dimer is  $\sim 120$  nm  $\times$  120 nm, double the width of a single tile. In the lower left of the micrograph, a zoomed dimer can be seen.

We found the yield of dimers to be strongly dependent on the  $Mg^{2+}$  concentration of the second step annealing process. Fig. 2 shows the AFM images of samples with varying amounts of  $Mg^{2+}$ . The yield of dimers was  $\sim 48\%$  (Fig. 2a) using the 1xTAE buffer with 12.5 mM  $Mg^{2+}$ . The yield of dimers increased with increasing  $Mg^{2+}$  concentration, to  $\sim 78\%$  with 30.0 mM  $Mg^{2+}$  (Fig. 2b), and to near quantitative when the  $Mg^{2+}$  concentration was increased further to 60.0 mM (Fig. 2c and S2 and S3). Herein, we introduce the magnesium dependent assembly of DNA origami with vertical linkers, this method will open an effective way to build large area of 2D

and 3D DNA origami nanostructures with both edges. It not only simplifies the DNA origami tile design, but also increases the effective surface area of DNA arrays to incorporate non-DNA nanomaterials for versatile applications.

To demonstrate the utility of this approach and to show that the top and bottom face of the double sized DNA origami are well defined, we positioned multiple inorganic nanomaterials (gold nanoparticles (AuNPs)) on the assembled origami dimers on both the top and bottom sides with precise positional control. Fig. 3a is a schematic of the locations of the sticky-ends on the dimer template used for the AuNP assembly. The sticky-ends at the four corners are represented by red solid circle point out of the plane of the page. The distance between two sites is  $\sim 80$  nm (256 nucleotides) along the duplex axis. Each binding site consists of three DNA sticky-ends extended from the selected staple strands on the DNA origami template. The length of the sticky-ends is 15 adenines. Four other modifications were made  $\sim 60$  nm (192 nucleotides) apart on the opposite side of the origami dimer (pointing into the plane of the page) and are shown in Fig. 3a as a green solid circle. Each binding site here consists of three DNA sticky-ends with 25 adenines.

The AuNPs, with a diameter of 5nm, were fully covered by thiolated DNA strands whose sequence is complementary to the sticky-ends on the origami template (see supplementary information for the sticky end sequences). Before the AuNP assembly, the dimers that formed with a  $Mg^{2+}$  concentration of 30.0 mM or 60.0 mM buffer were exchanged to 1  $\times$  TAE 12.5 mM  $Mg^{2+}$  through column filtration. The lower salt concentration is required to prevent aggregation of the AuNPs. A schematic drawing of assembly of AuNPs on double-side origami dimer is shown in Fig. 3b. Both single-sided and template double-sided attachments of AuNPs to the DNA origami were characterized by AFM. In Fig. 3c, the AFM image shows the AuNPs assembly on four corners when the DNA

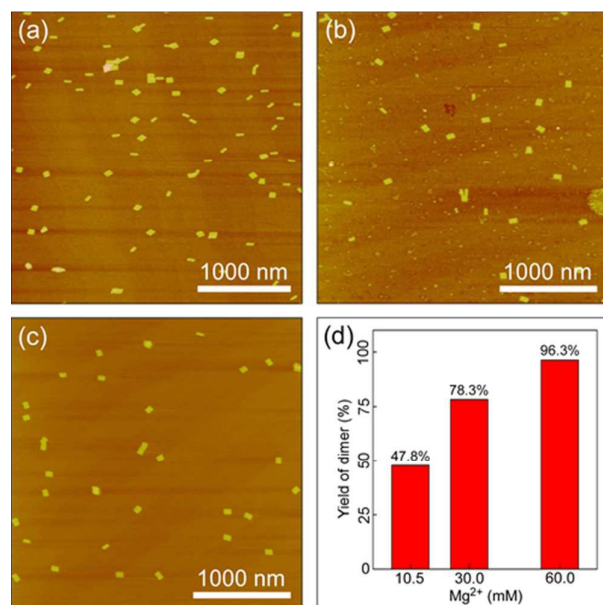


**Fig.2** Self-assembly of rectangle origami dimers with vertical linkers in different magnesium buffer concentrations. (a-c) AFM images of assembled dimers with (a) 10.5 mM Mg<sup>2+</sup> buffer. (b) The salt concentration of 30.0 mM and (c) 60.0 mM Mg<sup>2+</sup>. (d) The yield of dimers is 47.8% (N=335 dimer, N=772 monomer), for (a), 78.3% (N=240 dimer, N=123 monomer) for (b) and 96.3% (N=413 dimer, N=33 monomer) for (c). The AFM images were scanned with tapping mode in air.

sticky-ends were protruding on only one face. Fig. 3d shows assembly of four nanoparticles on the other side of the origami

dimer. The center-to-center distances between the particles along the duplex direction in the origami tile is  $81.5 \pm 4.6$  nm (40 measurements) in Fig. 3c and  $64.1 \pm 6.1$  nm (40 measurements) in Fig. 3d. These distances are consistent with the distance between the sticky ends in the origami. The efficiency of binding four AuNPs to different sides of origami was calculated based on the scanned AFM images. Fig. S4a shows histograms of the number of AuNPs attached to DNA origami dimer with four center binding sites (25 adenines). The attachment yield for four AuNPs is around 74% and  $\sim 21\%$  for three particles. Fig. S4b shows the histograms of the number of AuNPs attached to DNA origami dimer with four corner binding sites (15 adenines) on the opposite side. The successful attachment yield of four AuNPs decreases to 28%, and the histogram peaks at 3 nanoparticles. The total binding yield of three and four AuNPs also can reach  $\sim 70\%$ . The higher attachment yield in the center versus the corners is primarily due to the different lengths of the sticky-ends used for binding at the different sites. The length at the center sites is 25 adenines, but it is 15 adenines at the corners. Extension of the length of the sticky-ends should dramatically increase the hybridization yield between origami template and the nanoparticles. However, we note also that two DNA origami tiles could share the AuNPs in the corner binding sites (Fig. 3c). Unfortunately, longer sticky-ends close to the edge of DNA templates are also likely to interfere with the dimerization.

Fig. 3e shows the AuNP assembly on the dimers containing double-side sticky-end linkers (zoomed images in fig. S5). The binding efficiency of AuNPs on the dimer was determined from AFM scans, shown in Fig. 4. We can see that the histogram peaked at 6 nanoparticles (33%) and the yield of eight particles attachment is only around 12%. The total binding yield of 6, 7

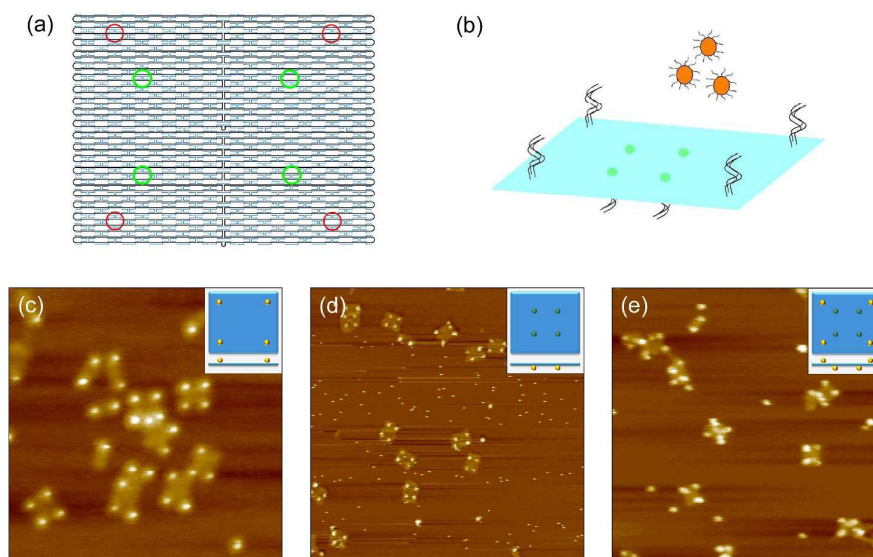


**Fig.3** Au nanoparticles assembly on both sides of the origami template. (a) Schematic showing locations of binding anchors. Anchors on the “top” and “bottom” of the origami are indicated by red solid outline circles and green solid outline circles, respectively. A 3D binding cartoon is shown in (b). (c) AFM image of Au nanoparticle assembly on one side of origami template at the four red circles anchors (scan area is  $1 \mu\text{m}$ ). (d) AFM image of Au nanoparticle assembly on one side of origami template at the four green circles anchors (scan area is  $1.5 \mu\text{m}$ ). (e) AFM image of Au nanoparticles assembly on both sides of the origami template, showing up to 8 AuNPs on a single scaffold (scan area is  $1.5 \mu\text{m}$ ).

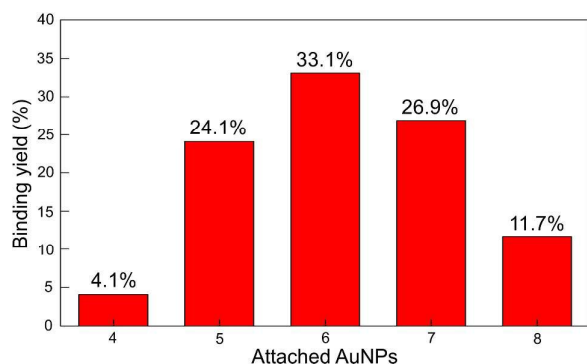


**Fig.4** Binding efficiency of AuNPs on opposite side of DNA origami dimer template. Data were collected from AFM image analysis of DNA origami dimer templates, N=145. The percent of 4 particles is 4.1%, 5 particles is 24.1%, 6 particles is 33.1%, 7 particles is 26.9%, 8 particles is 11.7%.

and 8 particles is > 70%.

DNA origami templates have been widely used to control the position of non-DNA materials. We have previously demonstrated the heterogeneous organization of both quantum dots and gold nanoparticles on opposite sides of a DNA origami scaffold.<sup>28</sup> This organization method was subsequently used to analyze the optical interaction between two/three nanoparticles by single-particle tracking methods.<sup>29</sup> The larger DNA surface associated with multiple nanoparticles presented here expands the range of assembly and could facilitate more complex particle-particle interactions.

In summary, we have presented a facile strategy to increase the connections between DNA origami tiles using vertical linkers. The key to achieving a high yield is increasing the concentration of Mg<sup>2+</sup> ions in the buffer solution. We anticipate that this method will be useful for the assembly higher-order DNA origami nanostructures that utilize both horizontal and vertical connections. In addition, we successfully assembled multiple AuNPs on opposite side of DNA origami dimer and found that the longer sticky-ends cohesion could increase the interaction between nanoparticles and origami template than the shorter ones. These results provide both a demonstration of a pathway to the self-assembly of large area DNA origami templates, and a demonstration of the feasibility of double-side modification of DNA origami scaffolds for more advanced applications.

We gratefully acknowledge financial support from the Office of Naval Research under Award N00014-09-1-1117. Additional support from the Nanoscale Science and Engineering Initiative of the National Science Foundation under NSF Award CHE-0641523 and from the New York State Office OF Science, Technology, and Academic Research (NYSTAR) is also gratefully acknowledged.

## Notes and references

1. P. W. Rothemund, *Nature*, 2006, **440**, 297-302.
2. Z. Zhao, H. Yan and Y. Liu, *Angewandte Chemie-International Edition*, 2010, **49**, 1414-1417.
3. Z. Zhao, Y. Liu and H. Yan, *Nano Letters*, 2011, **11**, 2997-3002.

4. Z. Li, M. H. Liu, L. Wang, J. Nangreave, H. Yan and Y. Liu, *Journal of the American Chemical Society*, 2010, **132**, 13545-13552.
5. W. Liu, H. Zhong, R. Wang and N. C. Seeman, *Angew Chem Int Ed Engl*, 2011, **50**, 264-267.
6. M. Endo, T. Sugita, A. Rajendran, Y. Katsuda, T. Emura, K. Hidaka and H. Sugiyama, *Chemical Communications*, 2011, **47**, 3213-3215.
7. A. Rajendran, M. Endo, Y. Katsuda, K. Hidaka and H. Sugiyama, *ACS Nano*, 2011, **5**, 665-671.
8. B. Q. Ding, Z. T. Deng, H. Yan, S. Cabrini, R. N. Zuckermann and J. Bokor, *Journal of the American Chemical Society*, 2010, **132**, 3248-+.
9. A. Kuzyk, R. Schreiber, H. Zhang, A. O. Govorov, T. Liedl and N. Liu, *Nature Materials*, 2014, **13**, 862-866.
10. X. Lan, Z. Chen, G. L. Dai, X. X. Lu, W. H. Ni and Q. B. Wang, *Journal of the American Chemical Society*, 2013, **135**, 11441-11444.
11. S. Pal, Z. T. Deng, H. N. Wang, S. L. Zou, Y. Liu and H. Yan, *Journal of the American Chemical Society*, 2011, **133**, 17606-17609.
12. W. Q. Shen, H. Zhong, D. Neff and M. L. Norton, *Journal of the American Chemical Society*, 2009, **131**, 6660-+.
13. K. Numajiri, M. Kimura, A. Kuzuya and M. Komiyama, *Chemical Communications*, 2010, **46**, 5127-5129.
14. H. T. Maune, S. P. Han, R. D. Barish, M. Bockrath, W. A. Goddard, P. W. K. Rothemund and E. Winfree, *Nature Nanotechnology*, 2010, **5**, 61-66.
15. A. P. Eskelinen, A. Kuzyk, T. K. Kaltiaisenaho, M. Y. Timmermans, A. G. Nasibulin, E. I. Kauppinen and P. Torma, *Small*, 2011, **7**, 746-750.
16. Z. Zhao, Y. Liu and H. Yan, *Organic & Biomolecular Chemistry*, 2013, **11**, 596-598.
17. A. Mangalum, M. Rahman and M. L. Norton, *Journal of the American Chemical Society*, 2013, **135**, 2451-2454.
18. Y. G. Ke, S. Lindsay, Y. Chang, Y. Liu and H. Yan, *Science*, 2008, **319**, 180-183.
19. H. Bui, C. Onodera, C. Kidwell, Y. Tan, E. Graugnard, W. Kuang, J. Lee, W. B. Knowlton, B. Yurke and W. L. Hughes, *Nano Letters*, 2010, **10**, 3367-3372.
20. R. Schreiber, J. Do, E. M. Roller, T. Zhang, V. J. Schuller, P. C. Nickels, J. Feldmann and T. Liedl, *Nature Nanotechnology*, 2014, **9**, 74-78.
21. H. Zhang, J. Chao, D. Pan, H. Liu, Q. Huang and C. Fan, *Chem Commun*, 2012, **48**, 6405-6407.
22. Y. Yang, D. Han, J. Nangreave, Y. Liu and H. Yan, *ACS Nano*, 2012, **6**, 8209-8215.
23. S. Woo and P. W. K. Rothemund, *Nature Communications*, 2014, **5**.
24. G. B. Yao, J. Li, J. Chao, H. Pei, H. J. Liu, Y. Zhao, J. Y. Shi, Q. Huang, L. H. Wang, W. Huang and C. H. Fan, *Angewandte Chemie-International Edition*, 2015, **54**, 2966-2969.
25. Y. Tian, T. Wang, W. Liu, H. L. Xin, H. Li, Y. Ke, W. M. Shih and O. Gang, *Nat Nanotechnol*, 2015, DOI: 10.1038/nnano.2015.105.
26. G. Tikhomirov, P. Petersen and L. Qian, *J Biomol Struct Dyn*, 2015, **33 Suppl 1**, 48-49.
27. T. Gerling, K. F. Wagenbauer, A. M. Neuner and H. Dietz, *Science*, 2015, **347**, 1446-1452.
28. R. Wang, C. Nuckolls and S. J. Wind, *Angew Chem Int Ed Engl*, 2012, **51**, 11325-11327.
29. S. H. Ko, K. Du and J. A. Liddle, *Angewandte Chemie-International Edition*, 2013, **52**, 1193-1197.